

Relativistic constituent quark model with infrared confinement

Tanja Branz¹, Amand Faessler¹, Thomas Gutsche¹, Mikhail A. Ivanov², Jürgen G. Körner³, Valery E. Lyubovitskij¹ *

¹ *Institut für Theoretische Physik, Universität Tübingen,
Kepler Center for Astro and Particle Physics,
Auf der Morgenstelle 14, D-72076 Tübingen, Germany*

² *Bogoliubov Laboratory of Theoretical Physics,
Joint Institute for Nuclear Research,
141980 Dubna, Russia*

³ *Institut für Physik, Johannes Gutenberg-Universität,
D-55099 Mainz, Germany*

(Dated: October 30, 2018)

We refine the relativistic constituent quark model developed in our previous papers to include the confinement of quarks. It is done, first, by introducing the scale integration in the space of α -parameters, and, second, by cutting this scale integration on the upper limit which corresponds to an infrared cutoff. In this manner one removes all possible thresholds presented in the initial quark diagram. The cutoff parameter is taken to be the same for all physical processes. We adjust other model parameters by fitting the calculated quantities of the basic physical processes to available experimental data. As an application, we calculate the electromagnetic form factors of the pion and the transition form factors of the ω and η Dalitz decays.

PACS numbers: 12.39.Ki,13.20.-v,13.25.-k,14.40.-n

Keywords: relativistic quark model, confinement, light and heavy mesons, strong, weak and electromagnetic decays

I. INTRODUCTION

The analysis of the structure of hadronic matter is one of the key tasks of modern particle physics. The generally accepted view is that hadrons are made up of the quark and gluon degrees of freedom of Quantum Chromo Dynamics (QCD) (see, e.g. the monograph [1]). An attempt to give a quantitative field theoretic description of hadrons and their interactions with quarks and gluons has to go beyond perturbation theory and necessarily implicates the use of nonperturbative methods. Such phenomena as hadronization, i.e. how hadrons are constructed from quarks, and confinement, the empirical fact that quarks have not been detected in isolation, can only be understood via non-perturbative methods. Significant progress has been made in constructing various quark models of hadrons which implement different features of QCD. For example, potential models provide simple tools that allow one to describe the hadron spectrum. However, the use of quantum mechanical potential models cannot explain the confinement of light quarks because quark creation and annihilation effects are essentially nonperturbative. In the approaches based on quantum field theory one can understand quark confinement as the absence of quark poles and thresholds in Green's functions and matrix elements.

In the Quark Confinement Model (QCM) Ref. [2] quark confinement was implemented by assuming that, at low energies, the constituent quark interacts with some given vacuum gluon configurations. As a result the quark has no fixed pole mass and there are no quark poles in the Green's functions and matrix elements. Models based on results obtained via QCD's Dyson-Schwinger equations (DSEs) [3] possess the feature that quark propagation is described by fully dressed Schwinger functions. Dressing of the quarks eliminates the threshold problem and thus one is effectively working with confined quarks. Using the framework of quantum field theory a promising approach for the description of composite particles as bound states of their constituents was suggested in [4].

Over the past years we have developed a relativistic constituent quark model and have applied the model to a large number of elementary particle processes [5]-[8]. The relativistic constituent quark model can be viewed as an effective quantum field approach to hadronic interactions based on an interaction Lagrangian of hadrons interacting with their constituent quarks. The coupling strength of the hadrons with the constituent quarks is determined by the compositeness condition $Z_H = 0$ [4] where Z_H is the wave function renormalization constant of the hadron. The

* On leave of absence from the Department of Physics, Tomsk State University, 634050 Tomsk, Russia

hadron field renormalization constant Z_H characterizes the overlap between the bare hadron field and the bound state formed from the constituents. Once this constant is set to zero, the dynamics of hadron interactions is fully described by constituent quarks in quark loop diagrams with local constituent quark propagators. Matrix elements are generated by a set of quark loop diagrams according to an $1/N_c$ expansion. The ultraviolet divergences of the quark loops are regularized by including vertex form factors for the hadron-quark vertices which, in addition, describe finite size effects due to the non-pointlike structure of hadrons. The relativistic constituent quark model contains only a few model parameters: the light and heavy constituent quark masses and the size parameters that describe the size of the distribution of the constituent quarks inside the hadron.

In the light quark sector this approach was successfully applied to describe the electromagnetic properties of the pion and the sigma meson [5], the electromagnetic form factors and magnetic moments of nucleons, and semileptonic decays of the light ground state baryon octet [6]. In the heavy quark sector we have calculated the baryonic Isgur-Wise functions, decay rates and asymmetry parameters for semileptonic decays of baryons, non-leptonic decay rates, and one-pion and one-photon transitions of heavy flavored baryons [7]. This technique was also applied to study the semileptonic decays of the double heavy baryons and the B_c -meson [8]. The same bound-state formalism was recently applied to the analysis of exotic hadron states –so-called hadronic molecules– in which the constituents are hadrons themselves rather than quarks as in the present approach [9].

The local form of the quark propagators used in the relativistic constituent quark model can lead to the appearance of threshold singularities corresponding to free quark production in transition amplitudes. As a result, applications of the relativistic quark model had to be restricted to ground state mesons and baryons with masses less than the sum of the constituent quark masses, and processes with relatively small energies. This poses problems for the description of e.g. light vector mesons, e.g. (ρ , K^*), and excited states where the particle mass exceeds the sum of the constituent quarks.

In the present work we propose a refinement of our previous quark model approach by effectively implementing quark confinement into the model. In the relativistic constituent quark model matrix elements are represented by a set of quark loop diagrams which are described by a convolution of the local quark propagators and vertex functions. By using Schwinger's α -representation for each local quark propagator and integrating out the loop momenta, one can write the resulting matrix element expression as an integral which includes integrations over a simplex of the α -parameters and an integration over a scale variable extending from zero to infinity. By introducing an infrared cutoff on the upper limit of the scale integration one can avoid the appearance of singularities in any matrix element. The new infrared cutoff parameter λ will be taken to have a common value for all processes. We determine the parameters of the model by a fit to available experimental data. As a first step, we apply our approach to evaluate the electromagnetic form factors of the pion and the transition form factors of the Dalitz decays $P \rightarrow \gamma l^+ l^-$ and $V \rightarrow P l^+ l^-$.

The paper is structured as follows. In Sec. II, we discuss the basic notions of the relativistic constituent quark model including a discussion on how gauge invariance is implemented in the model. We then go on to explain how to effectively implement infrared confinement. In Sec. III we determine the model parameters by a fit to the decay constants of the π and ρ mesons and then apply the covariant constituent quark model to evaluate the decays $\pi^0 \rightarrow \gamma \gamma$ and $\rho \rightarrow \pi \gamma$ including also the form factor behavior of the electromagnetic transitions. In Sec. IV, we extend our approach to the strange, charm and bottom sectors. We calculate the leptonic decay constants of both pseudoscalar and vector mesons, and the electromagnetic and leptonic decay widths. We calculate transition form factors and the widths of their Dalitz decays, and compare the results with recent experimental data. Finally, in Sec. V, we summarize our results. In Appendix A we describe in some technical detail how the one-loop integrations involving tensor loop momenta have been done. In Appendix B we proof by explicit calculation that the $\rho \rightarrow \gamma$ transition matrix element discussed in the main text is gauge invariant.

II. THEORETICAL FRAMEWORK

A. Lagrangian

The relativistic constituent quark model is based on an effective interaction Lagrangian describing the coupling of hadrons to their constituent quarks. In this paper we limit ourselves to the meson sector in which mesons are described as quark-antiquark bound states. An extension of the model to baryons (three-quark states) and multi-quark states is straightforward. The coupling of a meson $M(q_1 \bar{q}_2)$ to its constituent quarks q_1 and \bar{q}_2 is described by the nonlocal Lagrangian

$$\mathcal{L}_{\text{int}}^{\text{str}}(x) = g_M M(x) \int dx_1 \int dx_2 F_M(x, x_1, x_2) \bar{q}_1(x_1) \Gamma_M \lambda_M q_2(x_2) + \text{h.c.} \quad (1)$$

Here, λ_M and Γ_M are Gell-Mann and Dirac matrices (or a string of Dirac matrices) chosen appropriately to describe the flavor and spin quantum numbers of the meson field $M(x)$. In the case of pseudoscalar mesons we introduce singlet-octet mixing with a mixing angle of $\theta_P = -18^\circ$, while the vector mesons are assumed to be ideally mixed. The vertex function $F_M(x, x_1, x_2)$ characterizes the finite size of the meson. To satisfy translational invariance the vertex function has to obey the identity $F_M(x + a, x_1 + a, x_2 + a) = F_M(x, x_1, x_2)$ for any given four-vector a . In the following we use a specific form for the vertex function which satisfies the above translation invariance relation. One has

$$F_M(x, x_1, x_2) = \delta^{(4)}(x - \sum_{i=1}^2 w_i x_i) \Phi_M\left((x_1 - x_2)^2\right) \quad (2)$$

where Φ_M is the correlation function of the two constituent quarks with masses m_1 and m_2 . The variable w_i is defined by $w_i = m_i/(m_1 + m_2)$ so that $w_1 + w_2 = 1$. In principle, the Fourier transform of the correlation function, which we denote by $\Phi_M(-l^2)$, can be calculated from the solutions of the Bethe-Salpeter equation for the meson bound states [3]. In Refs. [5] it was found that, using various forms for the vertex function, the basic hadron observables are insensitive to the details of the functional form of the hadron-quark vertex form factor. We will use this observation as a guiding principle and choose a simple Gaussian form for the vertex function $\Phi_M(-l^2)$. The minus sign in the argument of $\Phi_M(-l^2)$ is chosen to emphasize that we are working in Minkowski space. One has

$$\Phi_M(-l^2) = \exp(l^2/\Lambda_M^2) \quad (3)$$

where the parameter Λ_M characterizes the size of the meson. Since l^2 turns into $-l^2$ in Euclidean space the form (3) has the appropriate fall-off behavior in the Euclidean region. We stress again that any choice for Φ_M is appropriate as long as it falls off sufficiently fast in the ultraviolet region of Euclidean space to render the Feynman diagrams ultraviolet finite.

In the evaluation of the quark-loop diagrams we use the free local fermion propagator for the constituent quark

$$S_q(k) = \frac{1}{m_q - \not{k} - i\epsilon} \quad (4)$$

with an effective constituent quark mass m_q . The local form of the quark propagator will lead to the appearance of threshold singularities corresponding to free quark production. It is for this reason that we had restricted previous applications of the relativistic quark model to the lowest-lying states that satisfy the condition $m_{q_1} + m_{q_2} > m_M$, and to processes with relatively low energies.

The coupling constant g_M in Eq. (1) is determined by the so-called *compositeness condition*. The compositeness condition requires that the renormalization constant Z_M of the elementary meson field $M(x)$ is set to zero, i.e.

$$Z_M = 1 - \Sigma'_M(m_M^2) = 0$$

where $\Sigma'_M(m_M^2)$ is the derivative of the mass operator corresponding to the self-energy diagram Fig. 1. One has

$$\Sigma'_M(m_M^2) = g_M^2 \Pi'_M(m_M^2) = g_M^2 \frac{d\Pi_M(p^2)}{dp^2} \Big|_{p^2=m_M^2} \quad (5)$$

and where m_M is the meson mass. At this point we take the mesons to be spinless for the sake of simplicity. The generalization to mesons (or baryons) with arbitrary spin is straightforward.

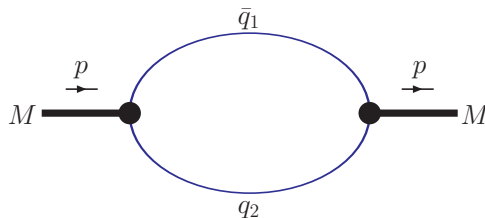


FIG. 1: Diagram describing the meson mass operator.

To clarify the physical meaning of the compositeness condition, we first want to remind the reader that the renormalization constant $Z_M^{1/2}$ can also be interpreted as the matrix element between the physical and the corresponding

bare state. For $Z_M = 0$ it then follows that the physical state does not contain the bare one and is therefore described as a bound state. The interaction Lagrangian Eq. (1) and the corresponding free Lagrangian describe both the constituents (quarks) and the physical particles (hadrons) which are bound states of the constituents. As a result of the interaction, the physical particle is dressed, i.e. its mass and wave function have to be renormalized. The condition $Z_M = 0$ also effectively excludes the constituent degrees of freedom from the space of physical states and thereby guarantees that there will be no double counting. The constituents exist in virtual states only. One of the corollaries of the compositeness condition is the absence of a direct interaction of the dressed charged particle with the electromagnetic field. Taking into account both the tree-level diagram and the diagrams with self-energy insertions into the external legs (that is the tree-level diagram times $Z_M - 1$) yields a common factor Z_M which is set to zero. This allows for another interpretation of the compositeness condition in as much as the condition $Z_M = 0$ leads to the correct normalization of the electric form factor of a charged particle at zero momentum transfer. By using the Ward identity which relates the electromagnetic vertex function at zero momentum transfer to the derivative of the mass operator for the on-mass-shell particle and taking into account the compositeness condition in the form of Eq. (5), one obtains

$$\Lambda^\mu(p, p) = \frac{d\Sigma_M(p^2)}{dp_\mu} = 2p^\mu \frac{d\Sigma_M(p^2)}{dp^2} = 2p^\mu. \quad (6)$$

$\Lambda^\mu(p, p)$ is the zero momentum transfer electromagnetic vertex function. The form (6) is more suitable for analytical calculations because the derivative of the mass operator with respect to p_μ determines the electromagnetic vertex function at zero momentum transfer.

B. Inclusion of photons

The interaction with the electromagnetic field is introduced in two stages. The free Lagrangian of quarks and hadrons is gauged in the standard manner by using minimal substitution:

$$\partial^\mu M^\pm \rightarrow (\partial^\mu \mp ieA^\mu)M^\pm, \quad \partial^\mu q \rightarrow (\partial^\mu - ie_q A^\mu)q, \quad \partial^\mu \bar{q} \rightarrow (\partial^\mu + ie_q A^\mu)\bar{q}, \quad (7)$$

where e is the positron (or proton) charge and where e_q is the quark's charge ($e_u = \frac{2}{3}e$, $e_d = -\frac{1}{3}e$, etc.). Minimal substitution gives us the first piece of the electromagnetic interaction Lagrangian

$$\begin{aligned} \mathcal{L}_{\text{int}}^{\text{em}(1)}(x) &= \sum_q e_q A_\mu(x) J_q^\mu(x) + e A_\mu(x) J_M^\mu(x) + e^2 A^2(x) M^-(x) M^+(x), \\ J_q^\mu(x) &= \bar{q}(x) \gamma^\mu q(x), \quad J_M^\mu(x) = i \left(M^-(x) \partial^\mu M^+(x) - M^+(x) \partial^\mu M^-(x) \right). \end{aligned} \quad (8)$$

It is important to reiterate that there is no direct coupling of the photon to the meson in our relativistic quark model due to the compositeness condition $Z_M = 0$ as has been emphasized in Sec. II A.

Gauging the nonlocal piece of the Lagrangian in Eq. (1) proceeds in a way suggested in [10]. In order to guarantee local gauge invariance of the strong interaction Lagrangian, one multiplies each quark field $q(x_i)$ in $\mathcal{L}_{\text{int}}^{\text{str}}$ with a gauge field exponential according to

$$\mathcal{L}_{\text{int}}^{\text{str+em}(2)}(x) = g_M M(x) \int dx_1 \int dx_2 F_M(x, x_1, x_2) \bar{q}_1(x_1) e^{ie_{q_1} I(x_1, x, P)} \Gamma_M \lambda_M e^{-ie_{q_2} I(x_2, x, P)} q_2(x_2), \quad (9)$$

where

$$I(x_i, x, P) = \int_x^{x_i} dz_\mu A^\mu(z). \quad (10)$$

It is readily seen that the full Lagrangian is invariant under the local gauge transformations

$$\begin{aligned} q_i(x) &\rightarrow e^{ie_{q_i} f(x)} q_i(x), & \bar{q}_i(x) &\rightarrow \bar{q}_i(x) e^{-ie_{q_i} f(x)}, & M(x) &\rightarrow e^{ie_M f(x)} M(x), \\ A^\mu(x) &\rightarrow A^\mu(x) + \partial^\mu f(x), \end{aligned} \quad (11)$$

where $e_M = e_{q_2} - e_{q_1}$ is the meson electric charge.

The second term of the electromagnetic interaction Lagrangian $\mathcal{L}_{\text{int};2}^{\text{em}}$ arises when one expands the gauge exponential in powers of A_μ up to the order of perturbation theory that one is considering. Superficially the results appear to depend on the path P which connects the end-points in the path integral in Eq (10). However, one needs to know only derivatives of the path integrals when doing the perturbative expansion. One can make use of the formalism developed in [10] which is based on the path-independent definition of the derivative of $I(x, y, P)$:

$$\lim_{dx^\mu \rightarrow 0} dx^\mu \frac{\partial}{\partial x^\mu} I(x, y, P) = \lim_{dx^\mu \rightarrow 0} [I(x + dx, y, P') - I(x, y, P)] \quad (12)$$

where the path P' is obtained from P by shifting the end-point x by dx . Use of the definition (12) leads to the key rule

$$\frac{\partial}{\partial x^\mu} I(x, y, P) = A_\mu(x) \quad (13)$$

which states that the derivative of the path integral $I(x, y, P)$ does not depend on the path P originally used in the definition. The non-minimal substitution (9) is therefore completely equivalent to the minimal prescription as is evident from the identities (12) or (13). The method of deriving Feynman rules for the non-local coupling of hadrons to photons and quarks was already developed in Refs. [5] and will be discussed in the next section where we apply the formalism to the physical processes considered in this paper.

For example, expanding the Lagrangian Eq. (9) up to the first order in A^μ one obtains ($l = w_1 p_1 + w_2 p_2$)

$$\begin{aligned} \mathcal{L}_{\text{int}}^{\text{em}(2)}(x) &= g_M M(x) \int dx_1 \int dx_2 \int dy E_M^\mu(x, x_1, x_2, y) A_\mu(y) \bar{q}_1(x_1) \Gamma_M \lambda_M q_2(x_2), \\ E_M^\mu(x, x_1, x_2, y) &= \int \frac{dp_1}{(2\pi)^4} \int \frac{dp_2}{(2\pi)^4} \int \frac{dq}{(2\pi)^4} e^{ip_1(x_1-x) - ip_2(x_2-x) + iq(y-x)} E_1^\mu(p_1, p_2, q), \\ E_1^\mu(p_1, p_2, q) &= -e_{q_1} w_1 (w_1 q^\mu + 2l^\mu) \int_0^1 dt \Phi'_H(-t(w_1 q + l)^2 - (1-t)l^2) \\ &\quad + e_{q_2} w_2 (w_2 q^\mu - 2l^\mu) \int_0^1 dt \Phi'_M(-t(w_2 q - l)^2 - (1-t)l^2), \end{aligned} \quad (14)$$

Let us emphasize that the vector Ward-Takahashi identity for an off-shell photon is also satisfied in this approach:

$$q_\mu \Lambda^\mu(p, p') = \Sigma_M(p^2) - \Sigma_M(p'^2), \quad (15)$$

where $\Lambda^\mu(p, p')$ is the meson electromagnetic vertex function described by the diagrams shown in Fig. 2. In order to guarantee the universality of neutral and charged current transitions (conserved vector current hypothesis) one also has to gauge the Lagrangian with regard to the electroweak interactions. This has been described in detail in Ref. [6] (see, also Sec. III).

C. Infrared confinement

Let us reiterate that the relativistic constituent quark model as described up to this point has a limited range of applications due to the threshold constraint $m_1 + m_2 > m_M$. In particular, processes involving light vector mesons, e.g. the ρ and K^* , and excited states cannot be treated within the model. In this section we extend the applicability of the relativistic constituent quark model by taking into account quark confinement effects. In order to elucidate how confinement is implemented in our framework we begin by considering a scalar one-pole propagator. The Schwinger representation of the propagator reads

$$\frac{1}{m^2 - p^2} = \int_0^\infty d\alpha \exp[-\alpha(m^2 - p^2)] \quad (16)$$

where the integration over the Schwinger parameter runs from 0 to ∞ . Instead of integrating to infinity we introduce an upper integration limit $1/\lambda^2$. We call the dimensional parameter λ (with mass dimension $[m]$) the infrared confinement

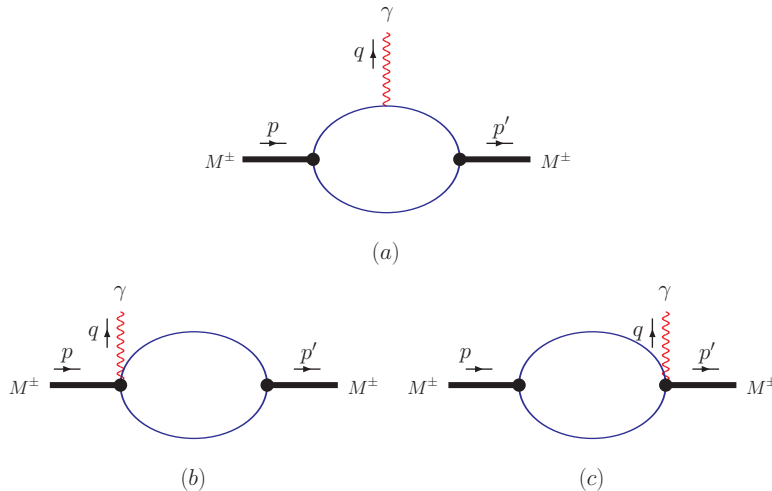


FIG. 2: Diagrams describing meson electromagnetic vertex function.

scale. By means of the cutoff one obtains an entire function which can be interpreted as a confined propagator,

$$\int_0^{1/\lambda^2} d\alpha \exp[-\alpha(m^2 - p^2)] = \frac{1 - \exp[-(m^2 - p^2)/\lambda^2]}{m^2 - p^2}. \quad (17)$$

Similar ideas have also been pursued in Refs. [11] where an infrared cutoff had been introduced in the context of a Nambu-Jona-Lasinio model. Note that the propagator for a particle in a constant self-dual field has a form similar to Eq. (17). Such vacuum gluon configurations have been studied in [12] and were then employed e.g. in [13] to construct a model with confined constituent quarks. The propagator in Eq. (17) does not have any singularities in the finite p^2 -plane, thus indicating the absence of a single quark in the asymptotic space of states.

However, the use of confined propagators in the form of entire functions has its own difficulties. The convolution of entire functions leads to a rapid growth of physical matrix elements once the hadron masses and energies of the reaction have been fixed. The numerical results become very sensitive to changes of the input parameters which requires extreme fine-tuning. For these reasons, we suggest to proceed in the following way.

Let us consider a general l -loop Feynman diagram with n propagators. One writes, using again the Schwinger parameterization,

$$\Pi(p_1, \dots, p_n) = \int_0^\infty d^n \alpha \int [d^4 k]^l \Phi \exp[-\sum_{i=1}^n \alpha_i (m_i^2 - p_i^2)] \quad (18)$$

where Φ stands for the numerator product of propagators and vertex functions. After doing the loop integrations one obtains

$$\Pi = \int_0^\infty d^n \alpha F(\alpha_1, \dots, \alpha_n), \quad (19)$$

where F stands for the whole structure of a given diagram. The set of Schwinger parameters α_i can be turned into a simplex by introducing an additional t -integration via the identity

$$1 = \int_0^\infty dt \delta(t - \sum_{i=1}^n \alpha_i) \quad (20)$$

leading to

$$\Pi = \int_0^\infty dt t^{n-1} \int_0^1 d^n \alpha \delta\left(1 - \sum_{i=1}^n \alpha_i\right) F(t\alpha_1, \dots, t\alpha_n). \quad (21)$$

As in Eq. (17) we cut off the upper integration at $1/\lambda^2$ and obtain

$$\Pi^c = \int_0^{1/\lambda^2} dt t^{n-1} \int_0^1 d^n \alpha \delta\left(1 - \sum_{i=1}^n \alpha_i\right) F(t\alpha_1, \dots, t\alpha_n) \quad (22)$$

By introducing the infrared cutoff one has removed all possible thresholds in the quark loop diagram. We take the cutoff parameter λ to be the same in all physical processes.

In order to make contact with recent ideas on the holographic description of particle interactions we change the integration variable t in Eq. (21) to z with $t = z^2$. One can then interpret z as an extra space coordinate and the upper integration limit $z_{\text{IR}} = 1/\lambda$ as the infrared scale where quarks are confined and hadronized. The analogy to the extra dimension holographic coordinate z introduced in holographic model is now apparent. We mention that the holographic model of hadrons is motivated by the anti-de Sitter/conformal field theory (AdS/CFT) correspondence, see Refs. [14]. There the truncation over the holographic coordinate z is necessary in order to break conformal invariance and to incorporate confinement in the infrared region.

As a further illustration of the infrared confinement effect relevant to the applications in this paper we consider the case of a scalar one-loop two-point function. One has

$$\Pi_2(p^2) = \int \frac{d^4 k_E}{\pi^2} \frac{e^{-sk_E^2}}{[m^2 + (k_E + \frac{1}{2}p_E)^2][m^2 + (k_E - \frac{1}{2}p_E)^2]} \quad (23)$$

where the numerator factor $e^{-sk_E^2}$ comes from the product of nonlocal vertex form factors of Gaussian form; k_E, p_E are Euclidean momenta. Doing the loop integration one obtains

$$\Pi_2(p^2) = \int_0^\infty dt \frac{t}{(s+t)^2} \int_0^1 d\alpha \exp\left\{-t[m^2 - \alpha(1-\alpha)p^2] + \frac{st}{s+t}\left(\alpha - \frac{1}{2}\right)^2 p^2\right\}. \quad (24)$$

The integral $\Pi_2(p^2)$ can be seen to have a branch point at $p^2 = 4m^2$. By introducing a cutoff in the t -integration one obtains

$$\Pi_2^c(p^2) = \int_0^{1/\lambda^2} dt \frac{t}{(s+t)^2} \int_0^1 d\alpha \exp\left\{-t[m^2 - \alpha(1-\alpha)p^2] + \frac{st}{s+t}\left(\alpha - \frac{1}{2}\right)^2 p^2\right\}, \quad (25)$$

where the one-loop two-point function $\Pi_2^c(p^2)$ no longer has a branch point at $p^2 = 4m^2$.

Such a confinement scenario can be realized with only minor changes in our approach by shifting the upper t -integration limit from infinity to $1/\lambda^2$. The confinement scenario also allows to include all possible resonance states in our calculations. First calculations done in this paper show that the limited set of adjustable parameters of the model (size parameters, constituent quark masses and the confinement scale λ) leads to a consistent description of a large number of low energy mesonic processes. We envisage a multitude of further applications as e.g. in the baryon sector.

III. BASIC PROPERTIES OF π AND ρ MESONS

In this section we discuss applications of the relativistic constituent quark model including infrared confinement to the decays of the π and ρ mesons. We start by fitting the model parameters. We calculate the leptonic constants f_π , $g_{\rho\gamma}$ and the electromagnetic couplings $g_{\pi\gamma\gamma}$ and $g_{\rho\pi\gamma}$. The relevant quark model diagrams are shown in Figs. 3 and 4. The corresponding Feynman one-loop integrals read:

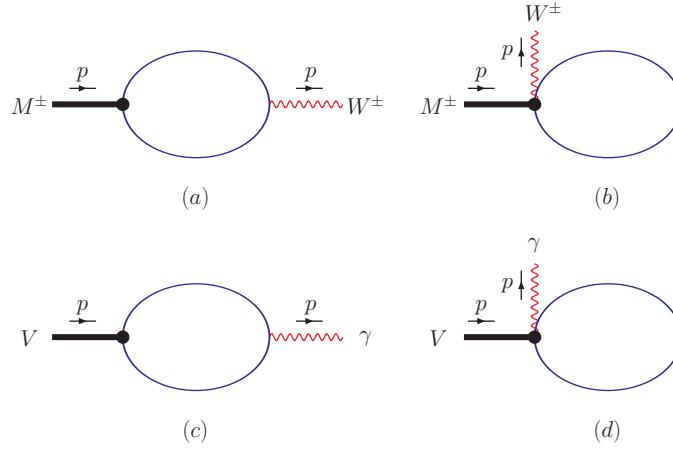


FIG. 3: Diagrams describing $M^\pm \rightarrow W^\pm$ (upper panel) and $V \rightarrow \gamma$ (lower panel) transitions.

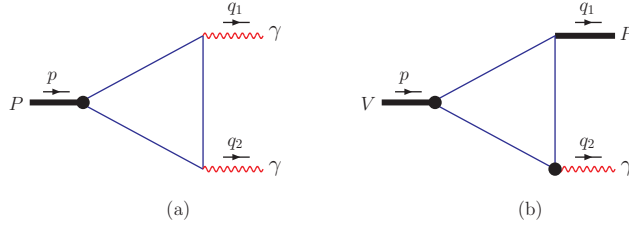


FIG. 4: Diagrams describing $P \rightarrow \gamma\gamma$ and $V \rightarrow P\gamma$ transitions.

$$\begin{aligned}
f_\pi p^\mu &= N_c g_\pi \int \frac{d^4 k}{(2\pi)^4 i} \left\{ \Phi_\pi(-k^2) \text{tr} \left[O^\mu S(k + \frac{1}{2}p) \gamma^5 S(k - \frac{1}{2}p) \right] \right. \\
&\quad \left. + \int_0^1 d\alpha \Phi'_\pi(-z_\alpha) (2k + \frac{1}{2}p)^\mu \text{tr} [S(k)] \right\}, \\
z_\alpha &= \alpha(k + \frac{1}{2}p)^2 + (1 - \alpha)k^2,
\end{aligned} \tag{26}$$

$$\begin{aligned}
g_{\rho\gamma} (g^{\mu\nu} p^2 - p^\mu p^\nu) &= \frac{N_c g_\rho}{\sqrt{2}} \int \frac{d^4 k}{(2\pi)^4 i} \left\{ \Phi_\rho(-k^2) \text{tr} \left[\gamma^\mu S(k + \frac{1}{2}p) \gamma^\nu S(k - \frac{1}{2}p) \right] \right. \\
&\quad \left. - \int_0^1 d\alpha \Phi'_\rho(-z_\alpha) (2k + \frac{1}{2}p)^\mu \text{tr} [\gamma^\nu S(k)] \right\},
\end{aligned} \tag{27}$$

$$g_{\pi\gamma\gamma} \epsilon^{\mu\nu q_1 q_2} = \frac{\sqrt{2} N_c}{3} \int \frac{d^4 k}{(2\pi)^4 i} \Phi_\pi(-k^2) \text{tr} \left[i\gamma^5 S(k + \frac{1}{2}p) \gamma^\mu S(k - \frac{1}{2}p) \gamma^\nu S(k + \frac{1}{2}p - q_1) \right], \tag{28}$$

$$\begin{aligned}
g_{\rho\pi\gamma} \epsilon^{\mu\nu q_1 q_2} &= \frac{N_c g_\rho g_\pi}{3} \int \frac{d^4 k}{(2\pi)^4 i} \Phi_\rho(-k^2) \Phi_\pi \left(-\left(k + \frac{1}{2}q_2\right)^2 \right) \\
&\quad \times \text{tr} \left[i\gamma^5 S(k + \frac{1}{2}p) \gamma^\mu S(k - \frac{1}{2}p) \gamma^\nu S(k + \frac{1}{2}p - q_1) \right],
\end{aligned} \tag{29}$$

where $N_c = 3$ is the number of colors, $O^\mu = \gamma^\mu(I - \gamma^5)$ is the left-chiral weak coupling matrix and the local propagators $S(k)$ etc. are defined in Eq. (4).

The meson-quark coupling constants are determined from the compositeness condition Eq. (6). This requires the evaluation of the derivative of the mass operator. For the pseudoscalar and vector mesons treated in this paper the

derivatives of the mass operators read

$$\begin{aligned}\Pi'_P(p^2) &= \frac{1}{2p^2} p^\alpha \frac{d}{dp^\alpha} N_c \int \frac{d^4k}{(2\pi)^4 i} \Phi_P^2(-k^2) \text{tr} \left[\gamma^5 S_1(k+w_1p) \gamma^5 S_2(k-w_2p) \right] \\ &= \frac{N_c}{2p^2} \int \frac{d^4k}{(2\pi)^4 i} \Phi_P^2(-k^2) \text{tr} \left[\gamma^5 S_1(k+w_1p) w_1 \not{p} S_1(k+w_1p) \gamma^5 S_2(k-w_2p) \right] + (m_1 \leftrightarrow m_2),\end{aligned}\quad (30)$$

$$\begin{aligned}\Pi'_V(p^2) &= \frac{1}{3} \left[g^{\mu\nu} - \frac{p^\mu p^\nu}{p^2} \right] \frac{1}{2p^2} p^\alpha \frac{d}{dp^\alpha} N_c \int \frac{d^4k}{(2\pi)^4 i} \Phi_V^2(-k^2) \text{tr} \left[\gamma^\mu S_1(k+w_1p) \gamma^\nu S_2(k-w_2p) \right] \\ &= \frac{1}{3} \left[g^{\mu\nu} - \frac{p^\mu p^\nu}{p^2} \right] \frac{N_c}{2p^2} \int \frac{d^4k}{(2\pi)^4 i} \Phi_V^2(-k^2) \text{tr} \left[\gamma^\mu S_1(k+w_1p) w_1 \not{p} S_1(k+w_1p) \gamma^\nu S_2(k-w_2p) \right] \\ &\quad + (m_1 \leftrightarrow m_2).\end{aligned}\quad (31)$$

Because of the the p^μ -derivative Eqs. (30) and (31) contain three propagator factors. The evaluation of the one-loop integrals Eqs. (26)–(31) proceeds as described in Appendix A.

There are four adjustable parameters: the constituent quark mass $m \equiv m_{u(d)}$, the size parameters Λ_π and Λ_ρ , and the scale parameter λ characterizing the infrared confinement. A least square fit to the observables yields the fit parameters

$$\begin{array}{ccccccc} & m & \Lambda_\pi & \Lambda_\rho & \lambda & & \\ \hline & 0.217 & 0.711 & 0.295 & 0.181 & \text{GeV} & \end{array}.\quad (32)$$

In Table I we compare the results of the fit with available experimental data.

TABLE I: Basic properties of the π and ρ meson.

Quantity	Our	Data [15]
f_π , MeV	130.2	$130.4 \pm 0.04 \pm 0.2$
$g_{\pi\gamma\gamma}$, GeV^{-1}	0.23	0.276
$g_{\rho\gamma}$	0.2	0.2
$g_{\rho\pi\gamma}$, GeV^{-1}	0.75	0.723 ± 0.037

As a first application of our approach we calculate the pion electromagnetic form factor F_π generated by the diagrams in Fig. 2, and the pion transition form factor $F_{\pi\gamma\gamma^*}$ generated by the diagram in Fig. 4(a). In the first case, we are interested in the space-like region $q^2 = -Q^2$. In the second case one photon is on-mass-shell $q_1^2 = 0$ and the second photon has a space-like momentum squared $q_2^2 = -Q^2$. The electromagnetic radii are related to the slope of form factors at the origin $r^2 = -6F'(0)$. Our result for the electromagnetic radius $r_\pi = 0.612$ fm is in good agreement with the present world average data of $r_\pi = (0.672 \pm 0.008)$ fm [15]. The result for the radius of the transition form factor $r_{\pi\gamma}^2 = 0.315$ fm² confirms the monopole-type approximation of the CLEO data [16] and is close to the CELLO measurement [17] of $r_{\pi\gamma}^2 = 0.42 \pm 0.04$ fm².

The electromagnetic pion transition form factor is displayed in Fig. 5 and compared with data from DESY [18], the Jefferson Lab F_π Collaboration [19] and the CERN NA7 Collaboration [20]. In Fig. 6 we display the $F_{\pi\gamma\gamma^*}(Q^2)$ form factor in the space-like region Q^2 up to 4 GeV².

Note that the slopes of the theoretical curves are quite sensitive to variations of the size parameter Λ_π . In order to exhibit the sensitivity to Λ_π we plot three curves for $\Lambda_\pi = 0.711, 1$ and 1.3 GeV in Fig. 5. Similarly, we display the sensitivity of the results on the infrared confinement scale for values of $\lambda = 0.010, 0.181$ and 0.200 GeV.

One should mention that our $F_{\pi\gamma\gamma^*}(Q^2)$ form factor behaves as $1/Q^2$ at large Q^2 in accordance with perturbative QCD. The calculated form factor behavior disagrees with the new data above 4 GeV² presented by the *BABAR* Collaboration [21]. For a recent theoretical analysis of the *BABAR* data, see e.g. Refs. [22].

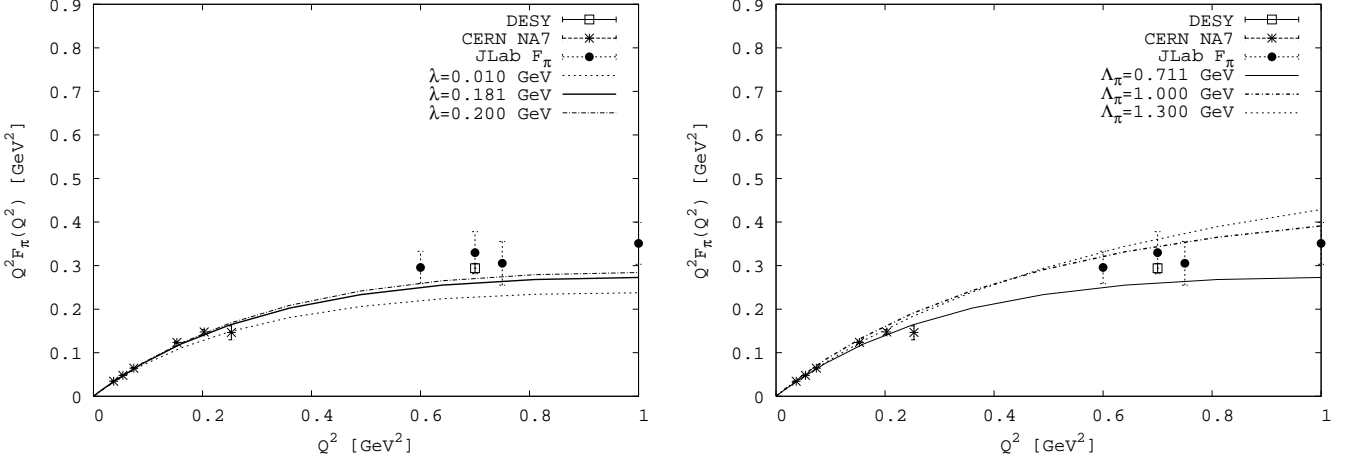


FIG. 5: Form factor $\pi^\pm \rightarrow \pi^\pm \gamma^*$ as function of the space-like photon momentum Q^2 . Data are taken from the JLAB F_π Collaboration [19], DESY [18] and CERN NA7 Collaboration [20].

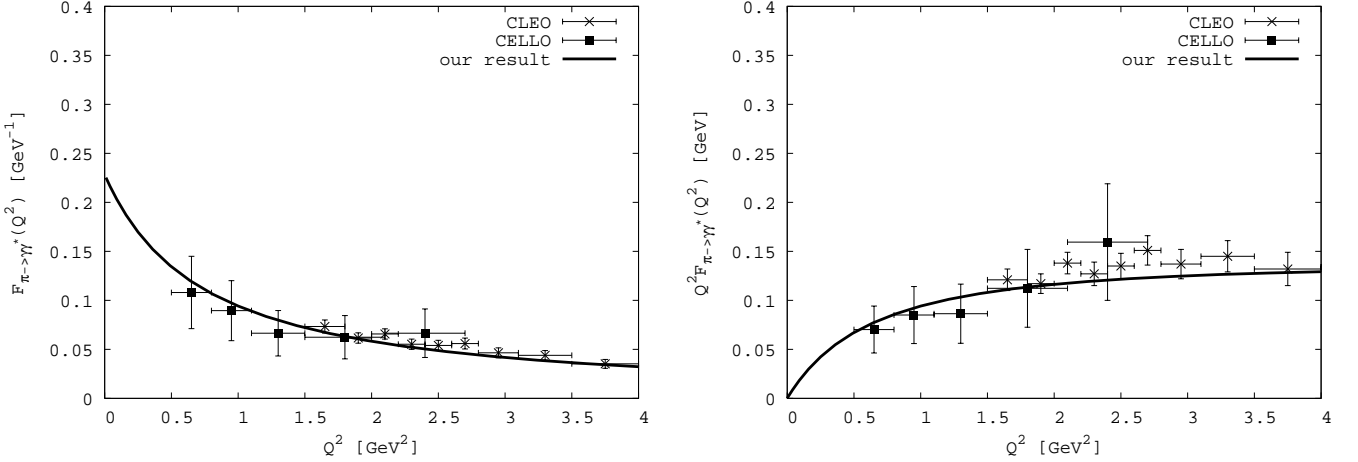


FIG. 6: Form factor $\gamma\gamma^* \rightarrow \pi^0$ as function of the space-like photon momentum Q^2 . Data are taken from CLEO [16].

IV. EXTENSION TO OTHER MESONS AND SOME APPLICATIONS

A. An extension to strange, charm and bottom flavors

In this subsection we extend our approach to mesons containing strange, charm and bottom quarks. We accordingly have to introduce a new set of fit parameters, namely, the values of constituent quark masses m_q ($q = s, c, b$) and the values of size parameters Λ_M for the corresponding mesons. Note that we keep the value of the confinement scale parameter λ fixed for all physical processes. For the fitting procedure we choose the weak and electromagnetic leptonic decay constants, see, Tables II-IV. We use the electromagnetic leptonic decay constants for the neutral vector mesons defined by $f_V = m_V g_{V\gamma}$ where the dimensionless constant $g_{V\gamma}$ was introduced in Sec. III by Eq. (27). Some comments should be done with respect to our fitting procedure. The values of strange, charm and bottom quark masses and of the size parameters of hadrons are determined by a least square fit to available experimental data for weak and electromagnetic leptonic decay constants shown in Tables II and III. In addition, we include the decays $\eta_c \rightarrow \gamma\gamma$ and $J/\psi \rightarrow \eta_c \gamma$ (see Table IV) for a better determination of the charm parameters. Since the size parameters $\Lambda_{J/\psi}$ and Λ_{η_c} are found to be close to each other we assume that the unknown value of Λ_{η_b} is approximately the same as Λ_Υ . The description of the η and η' mesons is more involved because both contain a non-strange and strange quark-antiquark admixture which is characterized by the mixing angle θ_P . Due to SU(3)-breaking we distinguish

between the size parameters of the non-strange and strange pieces of the quark current, i.e.

$$\begin{aligned}
\eta &\longrightarrow -\frac{1}{\sqrt{2}} \sin \delta \Phi_{\Lambda_\eta} (\bar{u}u + \bar{d}d) - \cos \delta \Phi_{\Lambda_{\eta_s}} \bar{s}s, \\
\eta' &\longrightarrow +\frac{1}{\sqrt{2}} \cos \delta \Phi_{\Lambda_{\eta'}} (\bar{u}u + \bar{d}d) - \sin \delta \Phi_{\Lambda_{\eta'_s}} \bar{s}s, \\
\delta &= \theta_P - \theta_I, \quad \theta_I = \arctan \frac{1}{\sqrt{2}}.
\end{aligned} \tag{33}$$

We use the experimental data of the electromagnetic decays involving η and η' (see Table IV) to fit the size parameters and the mixing angle. It appears that the best value for the mixing angle θ_P is -18° . This result is consistent with the range of values between -10° and -20° [15] obtained in direct extractions of θ_P from decay data involving η and η' . A mixing angle of or very close to -18° is also found in a direct analysis of the ratio $\Gamma(\eta' \rightarrow 2\gamma)/\Gamma(\eta \rightarrow 2\gamma)$ [15] or of tensor meson decay widths [26]. The least square fit yields the fit parameters:

$$\frac{m_s \quad m_c \quad m_b}{0.360 \quad 1.6 \quad 4.8 \quad \text{GeV}}. \tag{34}$$

$$\frac{\Lambda_{\rho/\omega/\phi} \quad \Lambda_\eta \quad \Lambda_\eta^s \quad \Lambda_{\eta'} \quad \Lambda_{\eta'}^s \quad \Lambda_K \quad \Lambda_{K^*} \quad \Lambda_D \quad \Lambda_{D^*} \quad \Lambda_{D_s} \quad \Lambda_{D_s^*} \quad \Lambda_{B/B^*} \quad \Lambda_{B_s/B_s^*} \quad \Lambda_{J/\psi} \quad \Lambda_{\eta_c/B_c} \quad \Lambda_\Upsilon \quad \Lambda_{\eta_b}}{0.295 \quad 0.70 \quad 0.85 \quad 0.27 \quad 0.45 \quad 0.87 \quad 0.30 \quad 1.4 \quad 2.3 \quad 1.95 \quad 2.6 \quad 3.35 \quad 4.4 \quad 3.3 \quad 3.0 \quad 5.07 \quad 5.0 \quad \text{GeV}} \tag{35}$$

In Tables II–IV we list the results of our numerical fit to the weak and electromagnetic leptonic decay constants

TABLE II: Weak leptonic decay constants $f_{P(V)}$ in MeV.

Meson	Our	Data [15]
π^-	130.2	$130.4 \pm 0.04 \pm 0.2$
K^-	155.4	$155.5 \pm 0.2 \pm 0.8$
D^+	206.2	205.8 ± 8.9
D_s^+	273.7	273 ± 10
B^-	216.4	216 ± 22
B_s^0	250.2	$253 \pm 8 \pm 7$
B_c	485.2	$489 \pm 5 \pm 3$ [23]
ρ^+	209.3	210.5 ± 0.6 [15]
D^{*+}	187.0	$245 \pm 20_{-2}^{+3}$ [24]
D_s^{*+}	213	$272 \pm 16_{-20}^{+3}$ [25]
B^{*+}	210.6	$196 \pm 24_{-2}^{+39}$ [24]
B_s^{*0}	264.6	$229 \pm 20_{-16}^{+41}$ [24]

together with their experimental values. Once the fit parameters are fixed one can use them to calculate a wide range of electromagnetic and dilepton decay widths. The results of the calculation are presented in Table IV which also includes experimental results whenever they are available.

Note that the electromagnetic properties of the π , K , ρ and ω mesons (form factors and radiative transitions) have also been considered in the light-front constituent quark model (LFCQM) developed in Ref. [27, 28]. It was shown that a reasonable description of data can be achieved with the use of the following values of the constituent quark masses $m_u = m_d = 220$ MeV and $m_s = 410$ MeV, which are close to our values $m_u = m_d = 217$ MeV and $m_s = 360$ MeV.

B. Dalitz decays

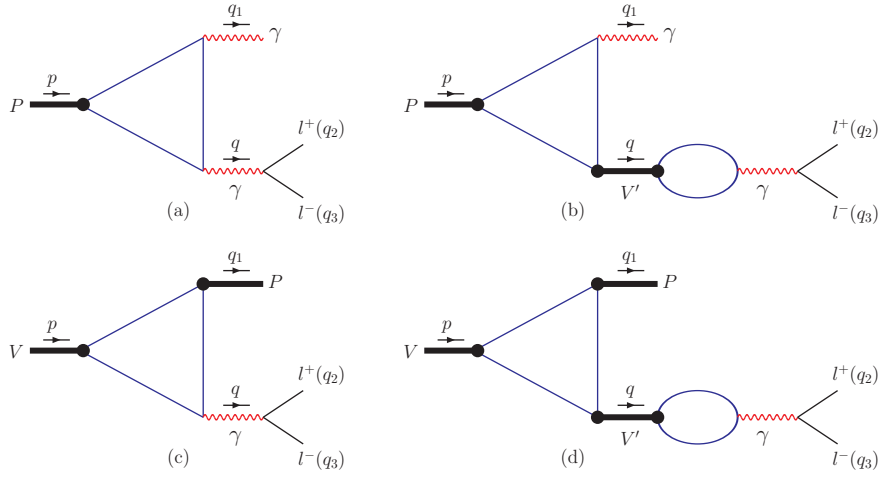
In this section we apply our approach to the Dalitz decays $P \rightarrow \gamma l^+ l^-$ and $V \rightarrow P l^+ l^-$ (for a theoretical review, see e.g. [29]). In particular, we analyze the transition form factors of the Dalitz decays $\eta \rightarrow \gamma \mu^+ \mu^-$ and $\omega \rightarrow \pi^0 \mu^+ \mu^-$

TABLE III: Electromagnetic leptonic decay constants f_V of vector mesons with hidden flavor in MeV.

Meson	Our	Data [15]
ρ^0	148.0	154.7 ± 0.7
ω	51.7	45.8 ± 0.8
ϕ	76.3	76 ± 1.2
J/ψ	277.4	277.6 ± 4
$\Upsilon(1s)$	238.4	238.5 ± 5.5

decays. Both form factors have been measured the SERPUKHOV-134 Collaboration (Protvino) [29] and recently by the NA60 experiment at the CERN SPS [30]. The $\omega \rightarrow \pi^0 \mu^+ \mu^-$ transition form factor has also been analyzed by the SND Collaboration at the BINP (Novosibirsk) [31].

The diagrams describing the Dalitz decays are shown in Fig. 7. They include both the diagrams with direct emission of the photon and resonance diagrams with an intermediate $V \rightarrow \gamma$ transition. Note, that such decays have been studied in [32] by using a similar relativistic quark model with confinement (Quark Confinement Model). The

FIG. 7: Diagrams describing the Dalitz decays $P \rightarrow \gamma l^+ l^-$ (upper panel) and $V \rightarrow P l^+ l^-$ (lower panel).

differential cross sections w.r.t. the dilepton mass squared $q^2 = (p_{l^+} + p_{l^-})^2$ reads (the data is usually plotted w.r.t. the dilepton mass $M = \sqrt{q^2}$, see e.g. [30])

$$\begin{aligned} \frac{d\Gamma(P \rightarrow \gamma l^+ l^-)}{dq^2} &= \frac{2}{3} \frac{\alpha}{\pi} \frac{\Gamma(P \rightarrow \gamma \gamma)}{q^2} \left(1 + \frac{2m_l^2}{q^2}\right) \left(1 - \frac{4m_l^2}{q^2}\right)^{1/2} \left(1 - \frac{q^2}{m_P^2}\right)^3 \\ &\times \left|F_P(q^2)\right|^2, \quad 4m_l^2 \leq q^2 \leq m_P^2, \end{aligned} \quad (36)$$

$$\begin{aligned} \frac{d\Gamma(V \rightarrow P l^+ l^-)}{dq^2} &= \frac{1}{3} \frac{\alpha}{\pi} \frac{\Gamma(V \rightarrow P \gamma)}{q^2} \left(1 + \frac{2m_l^2}{q^2}\right) \left(1 - \frac{4m_l^2}{q^2}\right)^{1/2} \left(1 - \frac{q^2}{(m_V - m_P)^2}\right)^{3/2} \left(1 - \frac{q^2}{(m_V + m_P)^2}\right)^{3/2} \\ &\times \left|F_V(q^2)\right|^2, \quad 4m_l^2 \leq q^2 \leq (m_V - m_P)^2. \end{aligned} \quad (37)$$

In our approach the normalized transition form factors are calculated in terms of the diagrams Fig. 7. The form

TABLE IV: Electromagnetic and leptonic decay widths in keV.

Process	Our	Data [15]
$\pi^0 \rightarrow \gamma\gamma$	5.40×10^{-3}	$(7.7 \pm 0.6) \times 10^{-3}$
$\eta \rightarrow \gamma\gamma$	0.51	0.510 ± 0.026
$\eta' \rightarrow \gamma\gamma$	4.27	4.28 ± 0.19
$\eta_c \rightarrow \gamma\gamma$	4.55	$7.2 \pm 0.7 \pm 2.0$
$\eta_b \rightarrow \gamma\gamma$	0.43	
$\rho^0 \rightarrow e^+e^-$	6.33	7.04 ± 0.06
$\omega \rightarrow e^+e^-$	0.76	0.60 ± 0.02
$\phi \rightarrow e^+e^-$	1.27	1.27 ± 0.04
$J/\psi \rightarrow e^+e^-$	5.54	$5.55 \pm 0.14 \pm 0.02$
$\Upsilon \rightarrow e^+e^-$	1.34	1.34 ± 0.018
$\rho^\pm \rightarrow \pi^\pm\gamma$	72.42	68 ± 7
$\rho^0 \rightarrow \eta\gamma$	63.25	62 ± 17
$\omega \rightarrow \pi^0\gamma$	682.71	703 ± 25
$\omega \rightarrow \eta\gamma$	7.63	6.1 ± 2.5
$\eta' \rightarrow \omega\gamma$	12.44	9.06 ± 2.87
$\phi \rightarrow \eta\gamma$	51.72	$58.9 \pm 0.5 \pm 2.4$
$\phi \rightarrow \eta'\gamma$	0.41	0.27 ± 0.01
$K^{*\pm} \rightarrow K^\pm\gamma$	40.86	50 ± 5
$K^{*0} \rightarrow K^0\gamma$	122.04	116 ± 10
$D^{*\pm} \rightarrow D^\pm\gamma$	0.62	1.5 ± 0.8
$D^{*0} \rightarrow D^0\gamma$	20.27	$< 0.9 \times 10^3$
$D_s^{*\pm} \rightarrow D_s^\pm\gamma$	0.30	$< 1.8 \times 10^3$
$B^{*\pm} \rightarrow B^\pm\gamma$	0.36	
$B^{*0} \rightarrow B^0\gamma$	0.12	
$B_s^{*0} \rightarrow B_s^0\gamma$	0.12	
$J/\psi \rightarrow \eta_c\gamma$	1.89	1.58 ± 0.37
$\Upsilon \rightarrow \eta_b\gamma$	0.02	

factors are given by

$$F_P(q^2) = \frac{1}{g_{P\gamma\gamma}} \times \left\{ g_{P\gamma\gamma}(q^2) + \sum_{V=\rho, \omega, \phi} g_{PV\gamma}(q^2) D_V(q^2) q^2 g_{V\gamma}(q^2) \right\}, \quad (38)$$

$$F_V(q^2) = \frac{1}{g_{VP\gamma}} \times \left\{ g_{VP\gamma}(q^2) + \sum_{V'=\rho, \omega, \phi} g_{VPV'}(q^2) D_{V'}(q^2) q^2 g_{V'\gamma}(q^2) \right\}. \quad (39)$$

The decay constants $g_{P\gamma\gamma} \equiv g_{P\gamma\gamma}(0)$ etc., are the same as defined in Sec. III. One has to note that if we assume that the quantities $g(q^2)$ in Eqs. (38) and (39) do not depend on q^2 then we reproduce the results of vector meson dominance (VMD).

The contributions of the intermediate vector meson resonances are described by a Breit–Wigner form where we have used a constant width in the imaginary part, i.e. we have used

$$D_V(q^2) = \frac{1}{m_V^2 - q^2 - im_V\Gamma_V}. \quad (40)$$

In Fig. 8 we plot the transition form factors for the two Dalitz decays $\eta \rightarrow \mu^+\mu^-\gamma$ and $\omega \rightarrow \pi^0\mu^+\mu^-$ measured by the

SERPUKHOV-134 Collaboration (Protvino) [29], the CERN NA60 Collaboration [30] and the SND Collaboration BINP (Novosibirsk) [31]. For completeness we also display our prediction for the Dalitz decay $\eta' \rightarrow \gamma e^+ e^-$ in comparison to the older data given in [29]. In Table V we present our results for the slope parameters defined by $F_X'(0)$.

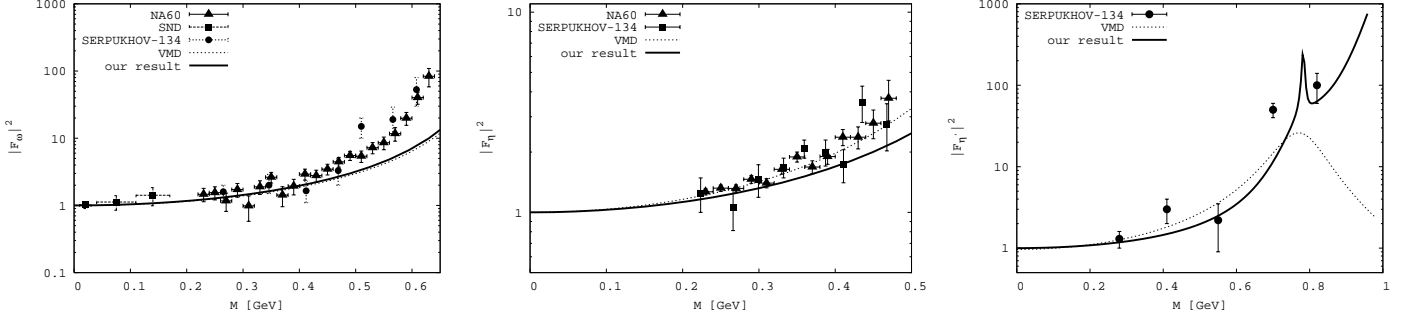


FIG. 8: The calculated form factors of the Dalitz decays $\omega \rightarrow \pi^0 l^+ l^-$, $\eta \rightarrow \gamma l^+ l^-$ and $\eta' \rightarrow \gamma l^+ l^-$ as functions of the dilepton mass $M = \sqrt{q^2}$. Experimental data are taken from [29, 30] for $\omega \rightarrow \pi^0 \mu^+ \mu^-$ and $\eta \rightarrow \gamma \mu^+ \mu^-$, from [31] for $\eta \rightarrow \gamma e^+ e^-$ and from [29] for $\eta' \rightarrow \gamma e^+ e^-$ (the five uncorrected by background points are included). For comparison we plot the VMD-curves.

Finally, our predictions for the Dalitz decay widths are given in Table VI. The agreement with the data is generally quite good except for the decay $\pi^0 \rightarrow \gamma e^+ e^-$ which comes out too small in our model. This is not unexpected since the decay $\pi^0 \rightarrow \gamma \gamma$ also comes out too small in our model (see Table IV).

TABLE V: Slope parameters of the Dalitz transition form factors in GeV^{-2} .

Decay mode	Our	Data
$\pi^0 \rightarrow \gamma l^+ l^-$	1.4	5.5 ± 1.6 [33]
$\eta \rightarrow \gamma l^+ l^-$	1.4	3 ± 1 [34]
		$1.95 \pm 0.17 \pm 0.05$ [30]
$\eta' \rightarrow \gamma l^+ l^-$	1.1	1.68 [35]
$\rho^0 \rightarrow \pi^0 l^+ l^-$	1.9	
$\omega \rightarrow \pi^0 l^+ l^-$	1.9	$2.24 \pm 0.06 \pm 0.02$ [30]
$\rho^0 \rightarrow \eta l^+ l^-$	2.2	
$\omega \rightarrow \eta l^+ l^-$	2.2	
$\phi \rightarrow \eta l^+ l^-$	1.4	
$\phi \rightarrow \eta' l^+ l^-$	2.5	

V. SUMMARY

We have refined a relativistic constituent quark model developed in our previous papers to include quark confinement effects. Quark confinement was implemented by introducing an upper cutoff on a scale integration which, in the original quark model, extends to infinity. The introduction of such an infrared cutoff removes all physical quark thresholds in the original quark diagrams. The cutoff parameter is taken to be the same for all physical processes. We adjust the model parameters by fitting the calculated quantities of the basic physical processes to available experimental data. As an application, we calculate the electromagnetic form factors of pion and the transition form factors of the Dalitz decays $P \rightarrow \gamma l^+ l^-$ and $V \rightarrow P l^+ l^-$. We extend our approach to mesons containing strange, charm and bottom quarks and calculate their leptonic and radiative decay constants.

TABLE VI: Dalitz decay widths in keV.

Decay mode	Our	Data [15]
$\pi^0 \rightarrow \gamma e^+ e^-$	6.4×10^{-5}	$(9.39 \pm 0.72) \times 10^{-5}$
$\eta \rightarrow \gamma e^+ e^-$	8.5×10^{-3}	$(8.84 \pm 1.14) \times 10^{-3}$
$\eta \rightarrow \gamma \mu^+ \mu^-$	0.4×10^{-3}	$(0.40 \pm 0.06) \times 10^{-3}$
$\eta' \rightarrow \gamma e^+ e^-$	9.0×10^{-2}	< 0.2
$\eta' \rightarrow \gamma \mu^+ \mu^-$	2.0×10^{-2}	$(3.2 \pm 1.2) \times 10^{-2}$
$\rho^0 \rightarrow \pi^0 e^+ e^-$	0.66	< 2.3
$\rho^0 \rightarrow \pi^0 \mu^+ \mu^-$	7.0×10^{-2}	
$\omega \rightarrow \pi^0 e^+ e^-$	6.23	6.54 ± 0.77
$\omega \rightarrow \pi^0 \mu^+ \mu^-$	0.65	0.82 ± 0.20
$\rho^0 \rightarrow \eta e^+ e^-$	0.46	< 1
$\omega \rightarrow \eta e^+ e^-$	5.6×10^{-2}	$< 9.3 \times 10^{-2}$
$\phi \rightarrow \eta e^+ e^-$	0.44	0.49 ± 0.04
$\phi \rightarrow \eta' e^+ e^-$	2.1×10^{-3}	
$\phi \rightarrow \eta \mu^+ \mu^-$	2.2×10^{-2}	$< 4 \times 10^{-2}$

Acknowledgments

We very much appreciate the help of Sanja Damjanovic and Hans Specht who provided us with the experimental data on the Dalitz decays. This work was supported by the DFG under Contract No. FA67/31-2 and No. GRK683. M.A.I. and J.G.K. appreciate the partial support of the Heisenberg-Landau program. The work of M.A.I. was supported by the DFG grant KO 1069/12-1. M.A.I. appreciates the support of Forschungszentrum "Elementarkräfte und mathematische Grundlagen". This research is also part of the European Community-Research Infrastructure Integrating Activity "Study of Strongly Interacting Matter" (HadronPhysics2, Grant Agreement No. 227431) and of the President grant of Russia "Scientific Schools" No. 3400.2010.2. The work is partially supported by Russian Science and Innovations Federal Agency under contract No. 02.740.11.0238.

Appendix A: Loop integration techniques

In order to demonstrate how the loop integrations are done consider a n -point one-loop diagram with n local propagators $S_i(k+v_i)$ and n Gaussian vertex functions $\Phi_i(-(k+v_{i+n})^2)$. In Minkowski space the one-loop diagram can be written as

$$I_n(p_1, \dots, p_n) = \int \frac{d^4 k}{\pi^{2i}} \text{tr} \prod_{i=1}^n \Phi_i(-(k+v_{i+n})^2) \Gamma_i S_i(k+v_i) \quad (\text{A1})$$

where the vectors v_i are linear combinations of the external momenta p_i to be specified in the following, k is the loop momentum, and the Γ_i are Dirac matrices (or strings of Dirac matrices) for the i th meson. The external momenta p_i are all chosen to be ingoing such that one has $\sum_{i=1}^n p_i = 0$. Due to translational invariance the integral Eq. (A1) is invariant under a shift of the loop momentum $k \rightarrow k+l$ by any four-vector l . The four-vector l may be any linear combination of the external momenta p_i .

Using the Schwinger representation of the local quark propagator one has

$$S_i(k+v_i) = (m_i + \not{k} + \not{v}_i) \times \int_0^\infty d\beta_i \exp[-\beta_i (m_i^2 - (k+v_i)^2)]. \quad (\text{A2})$$

For the vertex functions one takes the Gaussian form. One has

$$\Phi_i(-(k+v_{i+n})^2) = \exp[\beta_{i+n} (k+v_{i+n})^2] \quad i = 1, \dots, n, \quad (\text{A3})$$

where the parameters $\beta_{i+n} = s_i = 1/\Lambda_i^2$ are related to the size parameters. The numerator factors $m_i + k + \not{v}_i$ can be replaced by a differential operator in the following manner:

$$\begin{aligned} I_n(p_1, \dots, p_n) &= \int \frac{d^4 k}{\pi^{2i}} \text{tr} \prod_{i=1}^n \int_0^\infty d\beta_i e^{-\beta_i m_i^2} (m_i + k + \not{v}_i) \times \exp \left\{ \sum_{i=1}^{2n} \beta_i (k + v_i)^2 \right\} \\ &= \int \frac{d^4 k}{\pi^{2i}} \text{tr} \prod_{i=1}^n \int_0^\infty d\beta_i e^{-\beta_i m_i^2} \left(m_i + \not{v}_i + \frac{1}{2} \not{\partial}_r \right) \times \exp \left\{ \beta k^2 + 2kr + \sum_{i=1}^{2n} \beta_i v_i^2 \right\} \end{aligned} \quad (\text{A4})$$

where $\beta = \sum_{i=1}^{2n} \beta_i$ and $r = \sum_{i=1}^{2n} \beta_i v_i$. Next one does the loop integration and moves the Gaussian $\exp(-r^2/\beta)$ to the left of the differential operator. By using the identity

$$-\frac{r^2}{\beta} + \sum_{i=1}^{2n} \beta_i v_i^2 = \frac{1}{\beta} \sum_{1 \leq i < j \leq 2n} \beta_i \beta_j (v_i - v_j)^2 \quad (\text{A5})$$

one obtains

$$\begin{aligned} I_n(p_1, \dots, p_n) &= \prod_{i=1}^n \int_0^\infty \frac{d\beta_i}{\beta^2} \times \exp \left\{ -\sum_{i=1}^n \beta_i m_i^2 + \frac{1}{\beta} \sum_{1 \leq i < j \leq 2n} \beta_i \beta_j (v_i - v_j)^2 \right\} \\ &\times \text{tr} \prod_{i=1}^n \Gamma_i \left(m_i + \not{v}_i - \frac{1}{\beta} \not{v} + \frac{1}{2} \not{\partial}_r \right). \end{aligned} \quad (\text{A6})$$

We have written a FORM [36] program that achieves the necessary commutations in a very efficient way. As described in the main text the set of Schwinger parameters β_i ($i = 1, \dots, n$) can be turned into a simplex by writing

$$\int_0^\infty d^n \beta F(\beta_1, \dots, \beta_n) = \int_0^\infty dt t^{n-1} \int d^n \alpha \delta \left(1 - \sum_{i=1}^n \alpha_i \right) F(t\alpha_1, \dots, t\alpha_n). \quad (\text{A7})$$

One then arrives at the final representation of the one-loop n-point diagram in the form

$$\begin{aligned} I_n(p_1, \dots, p_n) &= \int_0^\infty dt \frac{t^{n-1}}{(s+t)^2} \int d^n \alpha \delta \left(1 - \sum_{i=1}^n \alpha_i \right) \exp \left\{ -t z_{\text{loc}} + \frac{st}{s+t} z_1 + \frac{s^2}{s+t} z_2 \right\} \\ &\times \text{tr} \prod_{i=1}^n \Gamma_i \left(m_i + \not{v}_i - \frac{1}{s+t} \not{v} + \frac{1}{2} \not{\partial}_r \right), \end{aligned} \quad (\text{A8})$$

where

$$\begin{aligned} z_{\text{loc}} &= \sum_{i=1}^n \alpha_i m_i^2 - \sum_{1 \leq i < j \leq n} \alpha_i \alpha_j A_{ij}, \\ z_1 &= \sum_{i=1}^n \alpha_i \sum_{j=n+1}^{2n} \bar{\beta}_j A_{ij} - \sum_{1 \leq i < j \leq n} \alpha_i \alpha_j A_{ij}, \\ z_2 &= \sum_{n+1 \leq i < j \leq 2n} \bar{\beta}_i \bar{\beta}_j A_{ij}, \\ r &= t \sum_{i=1}^n \alpha_i v_i + s \sum_{i=n+1}^{2n} \bar{\beta}_i v_i. \end{aligned}$$

Here, $\bar{\beta}_{i+n} = s_i/s$, $s = \sum_{i=1}^n s_i$. The matrix $A_{ij} = (v_i - v_j)^2$ ($1 \leq i, j \leq 2n$) depends on the invariant variables of the process.

There are altogether n numerical integrations, $n - 1$ α -parameter integrations and the integration over the scale parameter t . For the derivative of the (two-point function) mass operator one has to do one more α -parameter integration due to the extra propagator which comes in after the differentiation. The integration of the derivative of the mass operator proceeds in analogy to the n point function case described in this Appendix. We mention that the correctness of the numerical integration procedure can be checked very conveniently by shifting the loop integration momentum by a fixed momentum four-vector. The numerical evaluations have been done by a numerical program written in the FORTRAN code.

Some further remarks are in order. The convergence of the loop integral Eq. (A8) is defined by the local α form z_{loc} . If $z_{\text{loc}} \leq 0$ the t -integration becomes divergent due to contributions from the large t -region. The large t -region corresponds to that region where the singularities of the diagram with its local quark propagators appear. However, as described before, if one introduces an infrared cutoff on the upper limit of the t -integration, all singularities vanish because the integral is now convergent for any value of the set of kinematical variables. Note that the one-loop integration techniques described in this appendix can be extended to an arbitrary number of loops in a straightforward manner. Of particular interest is the extension to the two-loop case needed for the description of baryon transitions.

Appendix B: Gauge invariance of the $\rho^0 \rightarrow \gamma$ transition

In this appendix we want to demonstrate by an explicit calculation that the transition amplitude $\rho^0 \rightarrow \gamma$ written down in Eq. (27) satisfies gauge invariance, i.e. that e.g. the on-shell photon has only two transverse degrees of freedom. According to the formalism developed in Sec. II B there are the two contributions to the transition $\rho^0 \rightarrow \gamma$. The first contribution results from the minimal substitution in the free quark Lagrangian and is depicted in Fig. 3(a). In Fig. 3(b) we depict the point interaction contribution resulting from gauging the nonlocal Lagrangian.

We begin by considering the transition of an on-shell ρ to an off-shell photon with invariant mass p^2 . The corresponding transition amplitude $M^{\mu\nu}(p)$ must satisfy the gauge invariance condition $p_\nu M^{\mu\nu}(p) = 0$ as has already been assumed in writing down Eq. (27). We shall now show by explicit calculation that the non-gauge invariant pieces in the two contributions cancel each other resulting in an overall gauge invariant contribution. First we isolate the non-gauge invariant pieces in the two respective contributions by writing

$$\begin{aligned} M_a^{\mu\nu}(p) &= \int \frac{d^4k}{4\pi^2 i} \Phi_\rho(-k^2) \text{tr} \left(\gamma^\mu S(k + \frac{1}{2}p) \gamma^\nu S(k - \frac{1}{2}p) \right) \\ &= g^{\mu\nu} \left[I_a^{(1)}(p^2) + I_a^{(2)}(p^2) \right] + (g^{\mu\nu} p^2 - p^\mu p^\nu) I_a^\perp(p^2). \end{aligned} \quad (\text{B1})$$

The non-gauge invariant contributions are given by

$$\begin{aligned} I_a^{(1)}(p^2) &= \int_0^\infty \frac{dt}{(s+t)^2} e^{-z_1}, \quad z_1 = tm^2 - \frac{st}{s+t} \frac{p^2}{4}, \\ I_a^{(2)}(p^2) &= \int_0^\infty \frac{dt t}{(s+t)^2} \int_0^1 d\alpha e^{-z_2} \left[-\frac{1}{s+t} + \frac{2t^2}{(s+t)^2} \left(\alpha - \frac{1}{2} \right)^2 p^2 \right], \\ z_2 &= t \left(m^2 - \alpha(1-\alpha)p^2 \right) - \frac{st}{s+t} \left(\alpha - \frac{1}{2} \right)^2 p^2, \end{aligned} \quad (\text{B2})$$

whereas the gauge invariant contribution is given by

$$I_a^\perp(p^2) = \int_0^\infty \frac{dt t}{(s+t)^2} \int_0^1 d\alpha e^{-z_2} \left[\frac{1}{2} - \frac{2t^2}{(s+t)^2} \left(\alpha - \frac{1}{2} \right)^2 \right]. \quad (\text{B3})$$

Similarly we have

$$\begin{aligned}
M_b^{\mu\nu}(p) &= - \int \frac{d^4 k}{4\pi^2 i} (2k + \frac{1}{2}p)^\mu \int_0^1 d\alpha \Phi'_\pi \left(-\alpha(k + \frac{1}{2}p)^2 - (1-\alpha)k^2 \right) \text{tr}(\gamma^\nu S(k)) \\
&= g^{\mu\nu} I_b^{(3)}(p^2) + (g^{\mu\nu} p^2 - p^\mu p^\nu) I_b^\perp(p^2), \\
I_b^{(3)}(p^2) &= \int_0^\infty \frac{dt s}{(s+t)^2} \int_0^1 d\alpha e^{-z_3} \left[-\frac{1}{s+t} - \left(1 - \frac{2s\alpha}{s+t}\right) \frac{s\alpha}{s+t} \frac{p^2}{4} \right], \\
I_b^\perp(p^2) &= \int_0^\infty \frac{dt s}{(s+t)^2} \int_0^1 d\alpha e^{-z_3} \frac{1}{4} \left(1 - \frac{2s\alpha}{s+t}\right) \frac{s\alpha}{s+t}, \quad z_3 = tm^2 - \left(1 - \frac{s\alpha}{s+t}\right) \frac{s\alpha}{4} p^2. \tag{B4}
\end{aligned}$$

Here $s = 1/\Lambda_\rho^2$. The non-gauge invariant pieces $I_a^{(1,2)}$ and $I_b^{(3)}$ cancel each other as can be seen by the following transformations. First, we note that the integrands of the integrals $I_a^{(2)}(p^2)$ and $I_b^{(3)}(p^2)$ may be expressed via the derivatives of z_2 and z_3 , respectively.

$$\begin{aligned}
I_a^{(2)}(p^2) &\longrightarrow -\frac{1}{s+t} + \frac{2t^2}{(s+t)^2} \left(\alpha - \frac{1}{2}\right)^2 p^2 = -\frac{1}{s+t} \left[1 - \left(\alpha - \frac{1}{2}\right) \frac{\partial z_2}{\partial \alpha} \right], \\
I_b^{(3)}(p^2) &\longrightarrow -\frac{1}{s+t} - \frac{p^2}{4} \left(1 - \frac{2\alpha s}{s+t}\right) \frac{\alpha s}{s+t} = -\frac{1}{s+t} \left[1 - \alpha \frac{\partial z_3}{\partial \alpha} \right].
\end{aligned}$$

The α -integration can be done by using the bound-state conditions $z_2(\alpha = 1) = z_2(\alpha = 0) = z_3(\alpha = 1) = z_1$. One obtains

$$\begin{aligned}
I_a^{(2)}(p^2) &= - \int_0^\infty \frac{dt t}{(s+t)^3} \int_0^1 d\left[\left(\alpha - \frac{1}{2}\right) e^{-z_2} \right] = - \int_0^\infty \frac{dt t}{(s+t)^3} e^{-z_1}, \\
I_b^{(3)}(p^2) &= - \int_0^\infty \frac{dt s}{(s+t)^3} \int_0^1 d\left[\alpha e^{-z_3} \right] = - \int_0^\infty \frac{dt}{(s+t)^3} e^{-z_1}
\end{aligned}$$

Finally, one has

$$I_a^{(1)}(p^2) + I_a^{(2)}(p^2) + I_b^{(3)}(p^2) = \int_0^\infty \frac{dt}{(s+t)^2} e^{-z_1} \left[1 - \frac{t}{s+t} - \frac{s}{s+t} \right] \equiv 0. \tag{B5}$$

The gauge invariance condition $p_\nu M^{\mu\nu}(p) = 0$ also guarantees that the longitudinal component of the photon decouples as $p^2 \rightarrow 0$.

-
- [1] A. W. Thomas and W. Weise, *The Structure of the Nucleon*, (Berlin, Germany, Wiley-VCH, 2001).
[2] G. V. Efimov and M. A. Ivanov, *The Quark Confinement Model of Hadrons*, (IOP Publishing, Bristol & Philadelphia, 1993).
[3] C. D. Roberts and S. M. Schmidt, Prog. Part. Nucl. Phys. **45**, S1 (2000) [arXiv:nucl-th/0005064].
[4] A. Salam, Nuovo Cim. **25**, 224 (1962); S. Weinberg, Phys. Rev. **130**, 776 (1963); for review, see K. Hayashi et al., Fort. Phys. **15**, 625 (1967).
[5] I. V. Anikin, M. A. Ivanov, N. B. Kulimanova and V. E. Lyubovitskij, Z. Phys. C **65**, 681 (1995); M. A. Ivanov and V. E. Lyubovitskij, Phys. Lett. B **408**, 435 (1997) [arXiv:hep-ph/9705423]; A. Faessler, T. Gutsche, M. A. Ivanov, V. E. Lyubovitskij and P. Wang, Phys. Rev. D **68**, 014011 (2003) [arXiv:hep-ph/0304031].

- [6] M. A. Ivanov, M. P. Locher and V. E. Lyubovitskij, *Few Body Syst.* **21**, 131 (1996); A. Faessler, T. Gutsche, B. R. Holstein, V. E. Lyubovitskij, D. Nicmorus and K. Pumsa-ard, *Phys. Rev. D* **74**, 074010 (2006) [arXiv:hep-ph/0608015]; A. Faessler, T. Gutsche, B. R. Holstein, M. A. Ivanov, J. G. Körner and V. E. Lyubovitskij, *Phys. Rev. D* **78**, 094005 (2008) [arXiv:0809.4159 [hep-ph]].
- [7] M. A. Ivanov, V. E. Lyubovitskij, J. G. Körner and P. Kroll, *Phys. Rev. D* **56**, 348 (1997) [arXiv:hep-ph/9612463]; M. A. Ivanov, J. G. Körner, V. E. Lyubovitskij and A. G. Rusetsky, *Phys. Rev. D* **57**, 5632 (1998) [arXiv:hep-ph/9709372]; *Phys. Rev. D* **60**, 094002 (1999) [arXiv:hep-ph/9904421]; *Phys. Lett. B* **442**, 435 (1998) [arXiv:hep-ph/9807519]; *Phys. Lett. B* **476**, 58 (2000) [arXiv:hep-ph/9910342]; M. A. Ivanov, J. G. Körner and V. E. Lyubovitskij, *Phys. Lett. B* **448**, 143 (1999) [arXiv:hep-ph/9811370]; A. Faessler, T. Gutsche, M. A. Ivanov, J. G. Körner and V. E. Lyubovitskij, *Phys. Lett. B* **518**, 55 (2001); *Phys. Rev. D* **80**, 034025 (2009) [arXiv:0907.0563 [hep-ph]]; A. Faessler, T. Gutsche, M. A. Ivanov, J. G. Körner, V. E. Lyubovitskij, D. Nicmorus and K. Pumsa-ard, *Phys. Rev. D* **73**, 094013 (2006) [arXiv:hep-ph/0602193].
- [8] M. A. Ivanov and P. Santorelli, *Phys. Lett. B* **456**, 248 (1999) [arXiv:hep-ph/9903446]; M. A. Ivanov, P. Santorelli and N. Tancredi, *Eur. Phys. J. A* **9**, 109 (2000) [arXiv:hep-ph/9905209]; M. A. Ivanov, J. G. Körner and P. Santorelli, *Phys. Rev. D* **63**, 074010 (2001) [arXiv:hep-ph/0007169]; *Phys. Rev. D* **70**, 014005 (2004) [arXiv:hep-ph/0311300]; *Phys. Rev. D* **73**, 054024 (2006) [arXiv:hep-ph/0602050]; *Phys. Rev. D* **71**, 094006 (2005) [Erratum-ibid. *D* **75**, 019901 (2007)] [arXiv:hep-ph/0501051]; A. Faessler, T. Gutsche, M. A. Ivanov, J. G. Körner and V. E. Lyubovitskij, *Eur. Phys. J. direct C* **4**, 18 (2002) [arXiv:hep-ph/0205287].
- [9] Y. Dong, A. Faessler, T. Gutsche, S. Kovalenko and V. E. Lyubovitskij, *Phys. Rev. D* **79**, 094013 (2009) [arXiv:0903.5416 [hep-ph]]; T. Branz, T. Gutsche and V. E. Lyubovitskij, *Phys. Rev. D* **79**, 014035 (2009) [arXiv:0812.0942 [hep-ph]]; *Phys. Rev. D* **78**, 114004 (2008) [arXiv:0808.0705 [hep-ph]]; T. Branz, T. Gutsche and V. E. Lyubovitskij, *Phys. Rev. D* **80**, 054019 (2009) [arXiv:0903.5424 [hep-ph]].
- [10] S. Mandelstam, *Annals Phys.* **19**, 1 (1962); J. Terning, *Phys. Rev. D* **44**, 887 (1991).
- [11] D. Ebert, T. Feldmann and H. Reinhardt, *Phys. Lett. B* **388**, 154 (1996) [arXiv:hep-ph/9608223]; M. K. Volkov and V. L. Yudichev, *Phys. Atom. Nucl.* **63**, 464 (2000) [*Yad. Fiz.* **63**, 536 (2000)].
- [12] H. Leutwyler, *Phys. Lett. B* **96**, 154 (1980).
- [13] G. V. Efimov and S. N. Nedelko, *Phys. Rev. D* **51** (1995) 176.
- [14] J. Erlich, E. Katz, D. T. Son and M. A. Stephanov, *Phys. Rev. Lett.* **95**, 261602 (2005) [arXiv:hep-ph/0501128]; A. Karch, E. Katz, D. T. Son and M. A. Stephanov, *Phys. Rev. D* **74**, 015005 (2006) [arXiv:hep-ph/0602229]; J. Polchinski and M. J. Strassler, *Phys. Rev. Lett.* **88**, 031601 (2002) [arXiv:hep-th/0109174]; G. F. de Teramond and S. J. Brodsky, *Phys. Rev. Lett.* **94**, 201601 (2005) [arXiv:hep-th/0501022]; S. J. Brodsky and G. F. de Teramond, *Phys. Rev. D* **77**, 056007 (2008) [arXiv:0707.3859 [hep-ph]].
- [15] C. Amsler *et al.* (Particle Data Group), *Phys. Lett. B* **667**, 1 (2008).
- [16] J. Gronberg *et al.* (CLEO Collaboration), *Phys. Rev. D* **57**, 33 (1998) [arXiv:hep-ex/9707031].
- [17] H. J. Behrend *et al.* (CELLO Collaboration), *Z. Phys. C* **49**, 401 (1991).
- [18] P. Brauel *et al.*, *Z. Phys. C* **3**, 101 (1979).
- [19] J. Volmer *et al.* (Jefferson Lab F(pi) Collaboration), *Phys. Rev. Lett.* **86**, 1713 (2001) [arXiv:nucl-ex/0010009].
- [20] S. R. Amendolia *et al.* (NA7 Collaboration), *Nucl. Phys. B* **277**, 168 (1986).
- [21] B. Aubert *et al.* (BABAR Collaboration), *Phys. Rev. D* **80**, 052002 (2009) [0905.4778 [hep-ex]].
- [22] A. E. Dorokhov, arXiv:0905.4577 [hep-ph]; A. V. Radyushkin, *Phys. Rev. D* **80**, 094009 (2009) [arXiv:0906.0323 [hep-ph]]; M. V. Polyakov, *JETP Lett.* **90**, 228 (2009) [arXiv:0906.0538 [hep-ph]].
- [23] T. W. Chiu and T. H. Hsieh (TWQCD Collaboration), *PoS LAT2006*, 180 (2007) [arXiv:0704.3495 [hep-lat]].
- [24] D. Becirevic, P. Boucaud, J. P. Leroy, V. Lubicz, G. Martinelli, F. Mescia and F. Rapuano, *Phys. Rev. D* **60**, 074501 (1999) [arXiv:hep-lat/9811003].
- [25] C. Aubin *et al.*, *Phys. Rev. Lett.* **95**, 122002 (2005) [arXiv:hep-lat/0506030].
- [26] C. Amsler and F. E. Close, *Phys. Rev. D* **53**, 295 (1996) [arXiv:hep-ph/9507326].
- [27] F. Cardarelli, I. L. Grach, I. M. Narodetsky, E. Pace, G. Salme and S. Simula, *Phys. Rev. D* **53**, 6682 (1996) [arXiv:nucl-th/9507038].
- [28] F. Cardarelli, I. L. Grach, I. Narodetsky, G. Salme and S. Simula, *Phys. Lett. B* **359**, 1 (1995) [arXiv:nucl-th/9509004].
- [29] L. G. Landsberg, *Phys. Rept.* **128**, 301 (1985).
- [30] R. Arnaldi *et al.* (NA60 Collaboration), *Phys. Lett. B* **677**, 260 (2009) [arXiv:0902.2547 [hep-ph]].
- [31] M. N. Achasov *et al.*, *J. Exp. Theor. Phys.* **107**, 61 (2008).
- [32] G. V. Efimov and M. A. Ivanov, *JETP Lett.* **32**, 55 (1980) [*Pisma Zh. Eksp. Teor. Fiz.* **32**, 60 (1980)]; M. Dineykhani, G. V. Efimov and M. A. Ivanov, *JETP Lett.* **33**, 62 (1981) [*Pisma Zh. Eksp. Teor. Fiz.* **33**, 66 (1981)]; G. V. Efimov, M. A. Ivanov and E. A. Nogovitsyn, *Sov. J. Nucl. Phys.* **34**, 149 (1981) [*Yad. Fiz.* **34**, 264 (1981)]; M. Dineykhani, G. V. Efimov and M. A. Ivanov, *Sov. J. Nucl. Phys.* **35**, 435 (1982). [*Yad. Fiz.* **35**, 748 (1982)].
- [33] J. Fischer *et al.*, *Phys. Lett. B* **73**, 359 (1978).
- [34] Yu. B. Bushnin *et al.*, *Phys. Lett. B* **79**, 147 (1978).
- [35] R. I. Dzhelyadin *et al.*, *Phys. Lett. B* **88**, 379 (1979).
- [36] J. A. M. Vermaseren, *Nucl. Phys. Proc. Suppl.* **183**, 19 (2008) [arXiv:0806.4080 [hep-ph]]; arXiv:math-ph/0010025.